JOURNAL OF MATERIALS SCIENCE **38** (2003) 2265–2270

A universal equivalent circuit model for the impedance response of composites

L. Y. WOO, S. WANSOM, A. D. HIXSON, M. A. CAMPO, T. O. MASON
Department of Materials Science and Engineering, Northwestern University, Evanston, IL 60208, USA

An equivalent circuit model has been developed to describe the impedance response of composites with insulating or conductive particles or fibers. Required inputs are the matrix conductivity, the "intrinsic conductivity" of the particles, and their volume fraction. The model has general applicability to systems involving moderately conductive matrices, insulating or conductive particles/fibers, and, in the case of conducting particles, the presence of a high impedance "coating" element on the particle surfaces. Ramifications for the use of impedance spectroscopy in the characterization of composite properties and the monitoring of their performance under load are discussed.

1. Introduction

There is recent evidence regarding the influence of inclusions (particles, fibers) on the AC impedance response of electrocomposites, including ceramic-matrix [1–3], cement-matrix composites [4–8], and even polymer-matrix systems [9] . This is in addition to extensive literature regarding the influence of conducting or insulating particles/fibers on the DC electrical properties of composites, e.g., as reviewed in [10–13]. While the effect of insulating particles on DC conductivity tends to be small (and negative), the effect of conducting particles on the AC conductivity can be quite pronounced (and positive), especially if fibers or similar objects with large aspect ratios (length divided by diameter) are involved.

It was recently demonstrated that conductive particle composites can exhibit unusual "dual arc" impedance behavior in Nyquist or −imaginary vs. +real impedance diagrams [1–3, 5–9]. For this to occur the matrix must be moderately conductive, the particles must be highly conductive, and a high impedance layer must exist at the particle surfaces. This layer can arise due to passive oxide film formation (e.g., on steel particles in cement matrices), electrochemical charge transfer resistance/double layers (e.g., on carbon particles in cement matrices), or Schottky barrier formation (e.g., between dissimilar semiconductors). A conceptual picture of this behavior is provided by the "frequency-switchable coating model [7]." At DC or low frequency AC excitation, the coating (film, layer, barrier) is intact, and the particles behave as if they are insulating with respect to the matrix. With increasing frequency, however, displacement currents through the coatings short out their high impedance, rendering the underlying particles conductive relative to the matrix. Typical impedance spectra exhibit two cusps (minimum absolute values of imaginary impedance)—one at the DC resistance of the composite (particles insulating) and one at the AC resistance of the composite (particles conductive).

Chung and coworkers have written extensively about potential applications of fiber-reinforced composites as "smart" materials, i.e., their capability for self-monitoring based upon changes in DC electrical properties [14–17]. The impedance response of such materials should provide complementary monitoring capabilities [18, 19]. An important step toward understanding and utilizing the impedance response of electrocomposites is the development of an equivalent circuit model for their behavior. The present work investigated model composites consisting of cement-matrices with insulating (glass) and conductive (steel) particles/fibers. The equivalent circuit developed to describe their impedance response is completely general and should apply to all composites fulfilling the criteria listed above.

2. Experimental procedure

Fiber-reinforced composites were prepared with type I ordinary Portland cement (OPC) at a water-to-cement ratio of 0.4 by weight. Steel fibers (2 mm long, 30 μm diameter) were dry-mixed with the cement powder by hand for 1 min. Water was then mixed in by hand for 3 min, after which the mixture was blended at high speed in a commercial blender for 2 min to achieve homogeneity. By magnetic separation and optical microscopy, a sampling of fibers from a similarly processed fresh paste showed no noticeable alteration in fiber geometry (i.e., bending or length changes) due to processing. Plain OPC specimens (without fibers) were mixed in a similar manner. Specimens were cast in rectangular polycarbonate molds (25 mm by 25 mm by 100 mm) with stainless steel electrodes (20 mm by

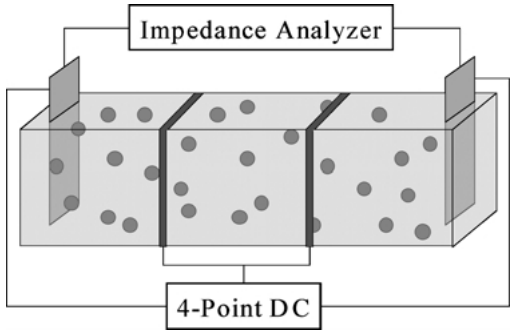

Figure 1 Experimental set-up for impedance and 4-point DC resistance measurements.

30 mm by 0.5 mm) cast in place approximately 5 mm from each end, producing an inter-electrode spacing of 90 mm. All samples were stored under 100% relative humidity (RH) during curing for 3 days.

Composites with spherical inclusions, steel ball bearings or glass beads, were similarly prepared from type I ordinary Portland cement (OPC) at a water-to-cement ratio of 0.4 by weight. The dry powder and water were mixed by hand for approximately 3 min prior to blending at high speed in a commercial blender for 2 min to achieve homogeneity. The slurries were allowed to set for an appropriate time (∼3 h) to achieve a viscosity sufficient to prevent subsequent settling by the steel ball bearings (3.18 mm diameter, Bearing Distributors, Wheeling, IL) or glass beads (3.0 mm diameter, Fox Industries, Fairfield, NJ), which were mixed in by hand. The viscous mixtures were then cast into rectangular polycarbonate molds (25 mm × 25 mm × 100 mm) with stainless steel electrodes (20 mm × 30 mm × 0.5 mm) cast in place 5 mm from each end (90 mm inter-electrode spacing), as in Fig. 1. Samples were cured under 100% RH for 7 days.

After curing, both fiber and particle composites were de-molded. The embedded steel electrodes served as 2-point impedance electrodes and as the current leads for 4-point DC resistance measurements. Voltage contacts for 4-point DC measurements were made by tightly wrapping 0.25 mm diameter steel wire loops around the samples, as shown in Fig. 1. Silver paste was painted over the wire loops in 2 mm wide strips to ensure electrical contact with the specimens. An enamel sealant was then used to seal the silver paste to prevent water (and contact) loss at these electrodes.

For 2-point impedance measurements, a Solartron 1260 impedance/gain-phase analyzer was employed with Z-60 personal computer software for data acquisition (Schlumberger, Houston, TX). The excitation voltage was 1 V and scans were performed from 11 MHz to 5 Hz, with data collected at 20 steps per frequency decade. The 4-point DC resistance measurements were carried out with a programmable current source and digital multimeter using LabVIEW personal computer software for data acquisition (Keithley, Models 220 and 2000, Cleveland, OH). For resistance measurements, current was applied to the outer electrodes of Fig. 1 in increments of 1 mA from 10 mA to –10 mA.

Equivalent circuit analysis was carried out using the "Equivalent Circuit" software program of Boukamp [20]. The simulation subroutine in this program is quite powerful and capable of simulating complex equivalent circuits involving resistors, capacitors, and so-called "complex phase elements" (see below).

3. Experimental results and analysis

Fig. 2a displays a typical result, plotted in terms of −imaginary vs. +real impedance (Nyquist representation), for a 0.35 vol% steel fiber-reinforced OPC composite vs. plain OPC. Fig. 3a shows typical results for composites with 20 vol% steel or glass spheres vs. plain OPC. To the right side (high impedance, low frequency) of each plot there is the start of a large electrode arc. It is well known that a highly resistive passive oxide film forms on steel electrodes when submerged in the high pH pore solution of OPC. For plain OPC and OPC with insulating inclusions there is a single point of minimum imaginary impedance (or rather the absolute value of imaginary impedance, which is negative in value). To the left of this point there is a single bulk arc. The shape of this arc does not change with the addition of insulating particles, but it shifts to the right (increased resistance, decreased conductivity). The bulk-electrode intersection agrees well with the 4-point DC resistance of the specimen in each case, within experimental error (±5%, based upon the uncertainty in geometric factors).

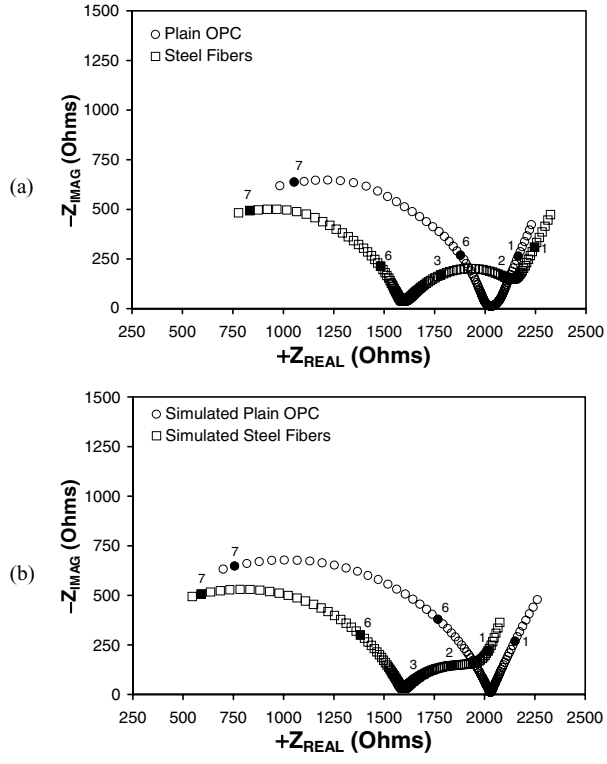

Figure 2 (a) Typical Nyquist plots for plain OPC and 0.35 vol% steel-reinforced OPC composite at 3 days, with frequency markers (log of frequency in Hz). (b) Simulated Nyquist plots for plain OPC and 0.35 vol% steel-reinforced OPC composite, with frequency markers. A dispersion factor of 0.26 was assumed (see the Appendix) and the following parameters were employed (Boukamp notation, see text): ([R(RQ)(RQ)][(RQ)(RQ)])(RQ) = 0.01 Ω, 7102 Ω, 2.9 × 10^{-10} F (0.75), 8 × 10^{5} Ω, 1.5 × 10^{-6} F (0.65), 2030 Ω, 1 × 10^{-9} F (0.75), 11.9 Ω, 1.7 × 10^{-7} F (0.85), 8 × 10^{3} Ω, 1.5 × 10^{-4} F (0.9), with n-values (see text Equations 8 and 9) in parentheses.

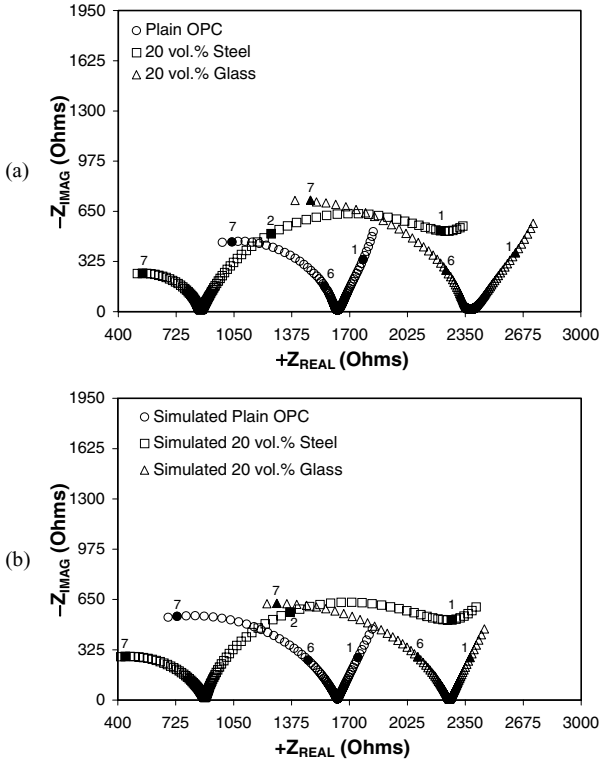

Figure 3 (a) Typical Nyquist plots for plain OPC and 20 vol% steel ball-reinforced or glass ball-reinforced OPC composites at 7 days, with frequency markers (log of frequency in Hz). (b) Simulated Nyquist plots for plain OPC and 20 vol% steel-reinforced OPC composite, with frequency markers. The following parameters were employed (Boukamp notation, see text): $([R(RQ)(RQ)][(RQ)(RQ))])(RQ) = 0.01$ or 10^9 Ω, 1469 Ω, 1.1×10^{-9} F (0.75), 5×10^6 Ω, 1.5×10^{-6} F (0.87), 1632 Ω, 1×10^{-9} F (0.75), 629 Ω, 2.6×10^{-9} F (0.65), 5×10^4 Ω, 1.5×10^{-4} F (0.75), with n-values (see text Equations 8 and 9) in parentheses.

On the other hand, the addition of conductive particles/fibers results in two bulk arcs with a distinct cusp between them. We hereafter refer to this point as the "cusp frequency" or "cusp resistance" (R_{cusp}). The intersection between rightmost bulk arc and the electrode arc is not as distinct, but agrees (within experimental error) with the 4-point DC resistance of each sample.

We have previously interpreted the behavior with conductive fibers in terms of a "frequency-switchable coating model" [7]. The basic outline is given in Fig. 4. R_{m} and C_{m} stand for the resistance and capacitance, respectively, of the matrix phase. R_{m}^* and C_{m}^* stand for the resistance and capacitance of inter-fiber regions along the "fiber" path. The same highly resistive passive oxide film that forms on the measurement electrodes also forms on individual steel fibers. At DC and low AC frequencies the oxide film isolates each fiber, effectively opening the "switch" in the lower path of Fig. 4b. Current flow through the surrounding matrix is relatively unaffected by the presence of the fiber, as shown by the dotted lines in Fig. 4a. As frequency increases, however, displacement currents through the oxide film short it out, the switch in Fig. 4b is "thrown", and the lower path dominates current flow as shown by the solid lines in Fig. 4a. Computer-generated gray-scale images of current flow under both conditions can be found in [7]. At DC the fiber appears black (no current), with a uniform gray level for the surrounding matrix. At the

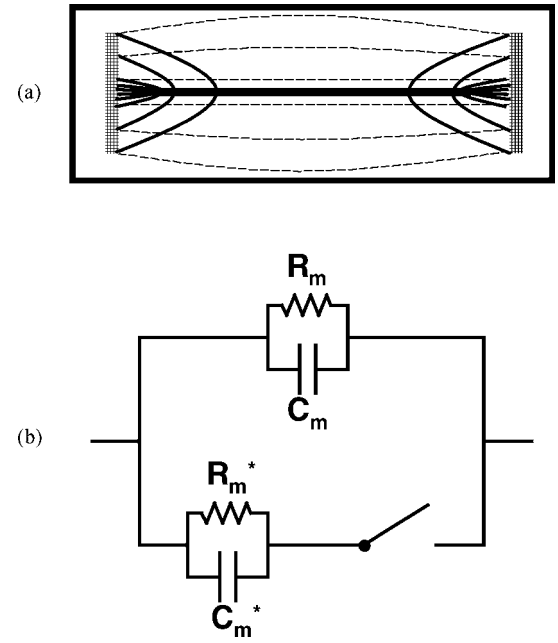

Figure 4 (a) Conceptual model for the current flow at DC (dotted lines) and at the cusp frequency under AC excitation (solid lines). (b) Equivalent circuit of the "frequency-switchable coating model" where R_{m} and C_{m} are the resistance and capacitance, respectively, of the matrix phase and R_{m}^* and C_{m}^* are the resistance and capacitance of inter-fiber regions along the "fiber" path.

cusp frequency the wire is white (high current), as is the matrix near the wire tips (current bunching), while the matrix surrounding the middle of the fiber is dark (little current here due to the matrix being bypassed by the fiber short-circuit path).

Although the equivalent circuit in Fig. 4 is conceptually adequate, it would be useful to have a more quantitative model to describe the impedance behavior of composites, including electrode effects (absent in Fig. 4). A more comprehensive equivalent circuit is shown in Fig. 5. The subscript "m" stands for matrix, whereas the subscript "c" stands for coating. Although application will be made to the steel-cement system, where the coating is a passive oxide film, the approach is completely general and can be readily extended to other types of systems. In all cases the subscript "p" stands for the particles/fibers. In the "circuit description code" (CDC) of Boukamp's program [20], the equivalent

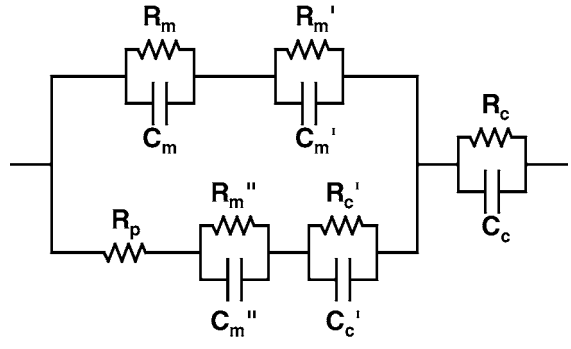

Figure 5 Comprehensive equivalent circuit model where the subscript "m" stands for the matrix, "c" for coating, and "p" for the particles/fibers. *R* and *C* are resistance and capacitance.

circuit of Fig. 5 is given by:

$$([R(RC)(RC)][(RC)(RC)])(RC) \quad (1)$$

where R = resistor, C = capacitor, and values are entered from left to right in the equivalent circuit, beginning with the lower "fiber" path, then the upper "matrix" path, and finally the electrode (the final (RC)) or coating element.

We begin by considering the situation involving insulating particles. The present simulations assumed $R_p = 10^9\ \Omega$, although any suitably high value of resistance can be used. This effectively eliminates the bottom "fiber" path from playing a role. Nevertheless, insulating particles can play a significant role in reducing conductivity (increasing resistance), as shown in Fig. 3a. Therefore, an additional $(R'_mC'_m)$ element is added in series to the matrix path in Fig. 5. The only requirement is that the time constants be identical, i.e., $(R'_mC'_m) = (R_mC_m)$, where R_m and C_m are the resistance and capacitance, respectively, of the matrix material, thereby resulting in a single bulk arc for the top path. To relate R'_m, or rather the sum of R'_m and R_m to particle/fiber volume fraction, we can employ the concept of "intrinsic conductivity". Based upon Maxwell's equation, Douglas and Garboczi [21] showed that in the dilute (low concentration) limit:

$$\sigma/\sigma_m = R_m/R = 1 + [\sigma]_\Delta\phi + 0(\phi^2) \quad (2)$$

where σ_m and R_m stand for the conductivity and resistance, respectively, of the matrix phase and σ and R stand for the conductivity and resistance, respectively, of the composite (in the present situation, $R = R_m + R'_m$). In Equation 2, ϕ is the volume fraction of particles, $[\sigma]_\Delta$ is the intrinsic conductivity, and higher order terms are neglected. Douglas and Garboczi tabulated and/or calculated intrinsic conductivities for a wide range of particle shapes in both the insulating ($\Delta = 0$) and conducting ($\Delta = \infty$) regimes. For example, spheres have intrinsic conductivities of $[\sigma]_0 = -3/2$ and $[\sigma]_\infty = +3$. Insulating right cylinders with aspect ratios (length divided by diameter) greater than 10 have an intrinsic conductivity of $[\sigma]_0 = -5/3$ [20]. Conducting right cylinders are more difficult to evaluate, but we recently reported a modified form of Fixman's equation [22, 23]:

$$[\sigma]_\infty = \frac{1}{3}\left(\frac{2(\mathrm{AR})^2}{[3\ln\{4(\mathrm{AR})\} - 7]} + 4\right) \quad (3)$$

where AR is aspect ratio, which estimates the intrinsic conductivity to within ±10%. It follows that fibers with large aspect ratios can have extremely high intrinsic conductivities in the conductive regime, resulting in large increases in conductivity (decreases in resistance) for small volume fraction additions, as shown in Fig. 2a.

Given the appropriate intrinsic conductivity of the dispersed particle and Equation 2, it can be shown that:

$$R'_m = \left(\frac{-[\sigma]_0\phi}{1 + [\sigma]_0\phi}\right)R_m \quad (4)$$

Since $[\sigma]_0$ values are negative, R'_m will be positive as anticipated. To maintain the $(R'_mC'_m) = (R_mC_m)$ time constant, C'_m is adjusted accordingly,

$$C'_m = \left(\frac{-[\sigma]_0\phi}{1 + [\sigma]_0\phi}\right)^{-1} C_m \quad (5)$$

In the case of conducting particles/fibers, R_p is given a negligibly small value (0.01 Ω in the present work). This activates the lower path in Fig. 5. Values of R'_c and C'_c are chosen to match the time constant of the electrode (R_cC_c), but with $R'_c \gg R_c$ (in the present work the best fits were achieved for R'_c approximately 100 times larger than R_c). This ensures that the lower path has high resistance at DC and low AC frequencies. Based upon Equation 2 and the appropriate intrinsic conductivities of the dispersed particles, it can be shown that:

$$R''_m = \left[\frac{1}{([\sigma]_\infty - [\sigma]_0)\phi}\right]R_m \quad (6)$$

The appearance of both intrinsic conductivities arises due to the necessity of the parallel R''_m to compensate for the increased resistance due to R'_m in the upper path. To maintain the $(R''_mC''_m) = (R_mC_m)$ time constant, C''_m is adjusted accordingly,

$$C''_m = [([\sigma]_\infty - [\sigma]_0)\phi]C_m \quad (7)$$

Successful simulations required the replacement of all capacitors in the equivalent circuit of Fig. 5 with constant phase elements (CPEs). The impedance function of a CPE is:

$$Z(\mathrm{CPE}) = B(j\omega)^{-n} \quad (8)$$

where B is a constant, ω is angular frequency, and n is a measure of arc-depression (θ):

$$n = 1 - 2\theta/\pi \quad (9)$$

For a perfect capacitor, $n = 1$ and B^{-1} is the capacitance. It can be seen that the experimental impedance arcs in Figs 2a and 3a are somewhat depressed below the real axis. We therefore obtained the best fit with the following CDC code:

$$([R(RQ)(RQ)][(RQ)(RQ)])(RQ) \quad (10)$$

while maintaining $(R'_mQ'_m) = (R_mQ_m)$, $(R''_mQ''_m) = (R_mQ_m)$, and n-values as given in the figure captions of Figs 2b and 3b. The values employed are consistent with typical values for plain OPC and the associated electrode arc (oxide film on steel) [5]. It should be stressed that we are fitting with three time-constants (bulk, oxide coating, electrode oxide), and the associated 9 adjustable parameters (R, Q, n for each type of element), which the three-arc spectra (two bulk arcs plus one electrode arc) will just allow.

Figs 2b and 3b show simulated impedance plots for the fiber-reinforced and spherical particle composites, respectively. In the case of spherical inclusions, the

agreement with the experimental results is quite good (Fig. 3b vs. a). By switching the value of R_p from 10^9 Ω (insulating particles/fibers) to 0.01 Ω (conducting particles/fibers), both situations in Fig. 3a were successfully simulated in Fig. 3b. In the case of conducting particles, the characteristic dual-arc (bulk) behavior was successfully obtained. The spherical particle composites had a loading level beyond the "dilute limit" ($\phi \sim 0.1$), so the intrinsic conductivity had to be corrected by the formula [24]:

$$[\sigma]_\infty = 3 + 4.5\phi + 5.25(\phi^2) \tag{11}$$

This points to the necessity of correcting intrinsic conductivities if outside the dilute limit. At the smaller loading levels for chopped fiber cement-based composites this should not be a problem.

The agreement between model and measured spectra is not as good for the fiber-reinforced composite (Fig. 2b vs. a). This may be due to incomplete dispersion of the fibers, i.e., fiber clumping. In separate work, we have developed a "dispersion factor" related to the degree of fiber dispersion in a given composite. A brief summary of this development is given in the Appendix. To make the "cusp" resistance in Fig. 2b agree with the experimental result in Fig. 2a, it was necessary to assume a dispersion factor of 0.26. This suggests that a high degree of fiber clumping is present (no dispersing agent was employed), which may likewise be responsible for the large arc depression evident in the experimental data. The influence of fiber clumping on the impedance response of fiber-reinforced composites is the subject of ongoing research.

The present work shows that it is possible to predict the impedance response of a composite with particles of arbitrary shape, as long as the intrinsic conductivities (insulating and conductive) are known and the volume fraction of particles is given. In the conductive regime the fibers must be highly conductive with respect to a moderately conductive matrix, and a high interfacial impedance is required. It must be stressed that particle dispersion must be homogeneous and random insofar as orientation (e.g., of fibers) is concerned. If so, the resulting composite properties should be isotropic. Impedance measurements vs. direction of applied field are a good test for isotropy in a given material.

Alternatively, deviations from predicted behavior can be used as a monitor for inhomogeneity and/or alignment problems (in the case of fibers, for example) caused by processing. Furthermore, deviations from predicted behavior or from that of as-prepared materials may prove useful for monitoring damage in composites under load or cyclic fatigue [18, 19].

4. Conclusions

A universal equivalent circuit model has been developed for a restricted class of composites. Given highly conductive particles/fibers, a moderately conductive matrix, and a high impedance "coating" (oxide film, charge transfer resistance/double layer, Schottky barrier, etc.) on the particles/fibers, a frequency-switchable coating effect allows for the particles/fibers to behave as if insulating at DC and low AC frequencies, but as if conducting at certain AC frequencies. Two bulk arcs are obtained in Nyquist (−imaginary vs. +real impedance) plots. The equivalent circuit consists of two bulk components in series, the latter accounting for the increased resistance due to the added "insulating" particles, which are in turn in parallel with a "particle" path consisting of particle resistance (can be high or low, to simulate insulating vs. conducting particles), a bulk component (to account for decreased resistance due to added "conducting" particles), and a coating element. The *RC* time constant of the coating element matches that of the external electrode element, but with a suitably higher resistance to eliminate the particle path at DC and low AC frequencies. The *RC* time constants of all three bulk components are identical. For cement-based composites, constant phase elements (CPEs) are employed to suitably model arc depression; *RC* elements are replaced by *RQ* elements, where *Q* represents a CPE. The circuit description code in Boukamp's formalism is given by ([*R*(*RQ*)(*RQ*)][(*RQ*)(*RQ*)])(*RQ*). Given the intrinsic conductivities of the particles/fibers employed, equations are provided to calculate all the requisite component values and successfully predict the impedance response of a given composite.

Acknowledgments

This work was supported by the National Science Foundation under grant no. DMR-00-73197 and made use of facilities of the Center for Advanced Cement-Based Materials.

Appendix

With well dispersed, highly conductive fibers, the matrix-normalized conductivity of a fiber-reinforced composite can be expressed as [21]:

$$\sigma/\sigma_m = R_m/R = 1 + [\sigma]_\Delta \phi \tag{A1}$$

where *m* stands for matrix, σ is conductivity, *R* is resistance, $[\sigma]_\Delta$ is the intrinsic conductivity of the fiber, and ϕ is its volume fraction. Since we are considering small volume fractions (e.g., 0.0035), higher order terms can be neglected. If fiber clumping takes place, Equation A1 must be modified to:

$$\sigma/\sigma_m = R_m/R = 1 + [\sigma]_\Delta \phi' + \sum [\sigma]_{\Delta i} \phi_i \tag{A2}$$

where ϕ' is the volume fraction of dispersed fibers and ϕ_i is the volume fraction of each specific type of fiber cluster having intrinsic conductivity $[\sigma]_{\Delta i}$. Subtracting 1 from both sides of Equations A1 and A2 and dividing, we obtain the "dispersion factor" as:

$$\mathrm{DF} = \left[\frac{\left(\frac{\sigma}{\sigma_m}\right)_{\text{composite}} - 1}{\left(\frac{\sigma}{\sigma_m}\right)_{\text{dispersed}} - 1} \right] = \frac{\phi'}{\phi} + \frac{\sum [\sigma]_{\Delta i} \phi_i}{[\sigma]_\Delta \phi} \tag{A3}$$

where the first term on the right side of the equation is the fraction of fibers which are dispersed in the matrix,

and the second term represents the contributions of all fiber clumps to the overall conductivity. We have considered clumps and clusters of various types, most of which result in significant decreases in intrinsic conductivity vs. that of isolated fibers. For example, a sheath of n fibers will have approximately the same effect on local current flow as a single fiber, but at n times the volume fraction; its intrinsic conductivity (for identical volume fraction) will be approximately n^{-1} that of isolated fibers ($[\sigma]_{\Delta}$).

In Equation A3 the composite (σ/σ_m) value is identical to the ratio, R_m/R, where R_m is the "cusp" resistance between the two bulk arcs (e.g., $\sim$1600 Ω in Fig. 2a) and either the bulk/electrode cusp for the composite or, preferably, the DC resistance of the plain matrix (e.g., $\sim$2050 Ω). The (σ/σ_m) value for the fully dispersed system can be calculated using Equation A1, based upon the volume fraction and the intrinsic conductivity of the fibers employed. In the present case, the aspect ratio was 67 (2 mm by 30 μm diameter) and the volume fraction was 0.35%. From text Equation 3 the intrinsic conductivity is estimated to be 308 and the conductivity ratio (σ/σ_m) should be 2.08. This is to be compared with the experimental value of 1.28 (2050 Ω/1600 Ω). The result is a "dispersion factor" of 0.26. It should be noted that this is not the fraction of dispersed fibers, but rather an upper limit for the fraction of dispersed fibers. The second term in Equation 3 may be significant or insignificant, depending upon the characteristics of the clumps/clusters formed and their individual intrinsic conductivities. A more thorough theoretical treatment of this impedance-based "dispersion factor" will be published separately.

References

1. C. A. WANG, Y. HUANG, Y. LI and Z. ZHANG, *J. Amer. Ceram. Soc.* **83** (2000) 2689.
2. R. GERHARDT and R. RUH, *ibid.* **84** (2001) 2328.
3. R. GERHARDT, J. RUNYAN, C. SANA, D. S. MCLACHLAN and R. RUH, *ibid.* **84** (2001) 2335.
4. P. GU, Z. XU, P. XIE and J. J. BEAUDOIN, *Cem. Concr. Res.* **23** (1993) 675.
5. S. J. FORD, J. D. SHANE and T. O. MASON, *ibid.* **28** (1998) 1737.
6. J. M. TORRENTS, T. O. MASON and E. J. GARBOCZI, *ibid.* **30** (2000) 585.
7. J. M. TORRENTS, T. O. MASON, A. PELED, S. P. SHAH and E. J. GARBOCZI, *J. Mater. Sci.* **36** (2001) 4003.
8. T. O. MASON, M. A. CAMPO, A. D. HIXSON and L. Y. WOO, *Cem. Concr. Comp.* **24** (2002) 457.
9. D. KAUSHIK, M. N. ALIAS and R. BROWN, *Corrosion* **47** (1991) 859.
10. R. LANDAUER, in "Electrical Transport and Optical Properties of Inhomogeneous Media," Vol. 40, edited by J. C. Garland and D. B. Tanner, AIP Conf. Proc. (American Institute of Physics, New York, 1978) p. 2.
11. R. E. MEREDITH and C. W. TOBIAS, in "Advances in Electrochemistry and Electrochemical Engineering," Vol. 2, edited by C. W. Tobias, (Interscience, New York, 1962) p. 15.
12. D. S. MCLACHLAN, M. BLASZKIEWICZ and R. E. NEWNHAM, *J. Amer. Ceram. Soc.* **73** (1990) 2187.
13. C.-W. NAN, *Prog. Mater. Sci.* **37** (1993) 1.
14. P.-W. CHEN and D. D. L. CHUNG, *J. Amer. Ceram. Soc.* **78** (1995) 816.
15. S. WAND and D. D. L. CHUNG, *Smart Mater. Struct.* **6** (1997) 199.
16. D. D. L. CHUNG, *Mater. Sci. Eng.* R **22** (1998) 57.
17. D. D. L. CHUNG, *J. Amer. Ceram. Soc.* **6** (2001) 75.
18. J. M. TORRENTS, T. C. EASLEY, K. T. FABER and T. O. MASON, *ibid.* **84** (2001) 740.
19. A. PELED, J. M. TORRENTS, T. O. MASON, S. P. SHAH and E. J. GARBOCZI, *ACI Mater. J.* **98** (2001) 313.
20. B. A. BOUKAMP, "Equivalent Circuit" (University of Twente, The Netherlands, 1990).
21. J. F. DOUGLAS and E. J. GARBOCZI, in "Advances in Chemical Physics," Vol. XCI, edited by I. Prigogine and S. A. Rice (John Wiley & Sons, 1995) p. 85.
22. M. FIXMAN, *J. Chem. Phys.* **75** (1981) 4040.
23. A. D. HIXSON, L. Y. WOO, M. A. CAMPO, T. O. MASON and E. J. GARBOCZI, *J. Electr.* **7** (2001) 189.
24. M. A. CAMPO, L. Y. WOO and T. O. MASON, *ibid.* **9** (2002) 49.

Received 9 July 2002
and accepted 12 February 2003